

Article

Exploring Transition from Stability to Chaos through Random Matrices

Roberto da Silva ^{1,2,*}  and Sandra Denise Prado ¹ ¹ Instituto de Física, Universidade Federal do Rio Grande do Sul, Porto Alegre 90010-150, RS, Brazil² Centro de Ciências Naturais e Humanas, Universidade Federal do ABC, Santo André 09210-580, SP, Brazil

* Correspondence: rasilva@if.ufrgs.br

Abstract: This study explores the application of random matrices to track chaotic dynamics within the Chirikov standard map. Our findings highlight the potential of matrices exhibiting Wishart-like characteristics, combined with statistical insights from their eigenvalue density, as a promising avenue for chaos monitoring. Inspired by a technique originally designed for detecting phase transitions in spin systems, we successfully adapted and applied it to identify analogous transformative patterns in the context of the Chirikov standard map. Leveraging the precision previously demonstrated in localizing critical points within magnetic systems in our prior research, our method accurately pinpoints the Chirikov resonance overlap criterion for the chaos boundary at $K \approx 2.43$, reinforcing its effectiveness. Additionally, we verified our findings by employing a combined approach that incorporates Lyapunov exponents and bifurcation diagrams. Lastly, we demonstrate the adaptability of our technique to other maps, establishing its capability to capture the transition to chaos, as evidenced in the logistic map.

Keywords: random matrices; chaos; monte carlo markov chain



Citation: Silva, R.d.; Prado, S.D. Exploring Transition from Stability to Chaos through Random Matrices. *Dynamics* **2023**, *3*, 777–792. <https://doi.org/10.3390/dynamics3040042>

Academic Editors: Christos Volos, Lazaros Moysis, Marcin Lawnik and Murilo da Silva Baptista

Received: 5 October 2023
Revised: 6 November 2023
Accepted: 7 November 2023
Published: 13 November 2023



Copyright: © 2023 by the authors. Licensee MDPI, Basel, Switzerland. This article is an open access article distributed under the terms and conditions of the Creative Commons Attribution (CC BY) license (<https://creativecommons.org/licenses/by/4.0/>).

1. Introduction

Chaotic behavior plays a crucial role in contemporary physics [1], as the comprehension of non-determinism under initial conditions arises in various contexts, including the stabilization of seemingly simple mechanical systems, such as the inverted pendulum [2,3].

The identification of chaos in specific Hamiltonian systems can be accomplished using traditional methods; however, there is room for the development of various alternatives. In contrast, the theory of random matrices has provided a robust and potent toolkit for describing several aspects of physical phenomena. This journey began with Wigner's pioneering work, which explained the intricate distribution of energies in heavy nuclei [4,5]. Subsequently, Dyson, displaying remarkable foresight, discerned that the joint distribution of eigenvalues in symmetric random matrices, characterized by well-behaved matrix entries, behaves analogously to a Coulomb gas of charged particles exhibiting logarithmic repulsion [6].

In recent times, the authors of this study have recognized the potential of a class of matrices known as Wishart-like matrices [7], demonstrating their successful application in characterizing the critical behavior of spin systems. This insight is revealed through the analysis of the spectra of these matrices, as presented in our prior works [8,9].

The concept revolves around considering a specified number of time evolutions of magnetization, acquired through a particular dynamics (e.g., Metropolis), as columns within matrices [8]. These rectangular matrices are then transformed into square matrices by multiplying the matrix by its transpose, wherein the eigenvalues of these matrices offer insights into the correlations among the time series data. Notably, phase transitions are associated with deviations from the Marchenko–Pastur eigenvalue density, which typically characterizes uncorrelated time series data [10].

This paper aims to investigate the relationship between time series generated through simple map iterations, exhibiting chaotic behavior, and the spectral properties of Wishart-like matrices constructed from these series. In essence, we sought to determine whether chaotic behavior is discernible in these spectra, thereby offering an alternative avenue for the study of chaotic phenomena

To accomplish this objective in our study, we opted for the Chirikov map iteration method [11,12]. This method's origins trace back to a particle subjected to the influence of a kicked potential, governed by a time-dependent Hamiltonian:

$$\mathcal{H}(q, p, t) = \frac{p^2}{2m} + K \cos q \sum_{n=0}^{\infty} \delta(t - n). \quad (1)$$

The dynamics consists of a sequence of free propagations interspersed with periodic kicks. The Hamiltonian equations yield:

$$\frac{dq}{dt} = \frac{\partial \mathcal{H}}{\partial p} = \frac{p}{m} \quad (2)$$

$$\frac{dp}{dt} = -\frac{\partial \mathcal{H}}{\partial q} = K \sin q \sum_{n=0}^{\infty} \delta(t - n)$$

Hence, the Chirikov standard map, which preserves the area in the phase space of the two canonical dynamical variables (q and p), is defined as follows:

$$\begin{aligned} p_{n+1} &= p_n + K \sin q_n \\ q_{n+1} &= q_n + p_{n+1}. \end{aligned} \quad (3)$$

We considered a unitary mass, $m = 1$, for which the dynamics can be visualized either within a cylinder by taking $q \bmod 2\pi$ or on a torus. In the latter scenario, we took $q \bmod 2\pi$ and $p \bmod 2\pi$.

From this interaction, we constructed square matrices and monitored their spectra as a function of K . Our findings indicated that the theoretical conjectures for the chaotic boundaries appear to be reflected in the minimal and maximal values of eigenvalue fluctuations (moments of eigenvalue density).

In the next section, we present a brief tutorial about random matrices with particular interest in Wishart-like matrices. We will show how the method worked to find the critical behavior of the Ising model and why it must work to find the chaotic behavior of the Chirikov map.

In the upcoming section, we offer a concise tutorial on random matrices, with a dedicated emphasis on Wishart-like matrices. We will delve into how this method has effectively revealed the critical behavior of the Ising model and why we hold the expectation that it will similarly shed light on the chaotic behavior of the Chirikov map. Following that, in Section 3, we present our primary findings. In Section 4, we conduct a supplementary validation of our method using the logistic map. Simultaneously, we observed that a fusion of bifurcation techniques and Lyapunov exponents yielded results consistent with our random-matrix-based approach for the Chirikov method.

Lastly, we draw our study to a close by summarizing our conclusions in Section 5.

2. Wishart-like Random Matrices: An Exploration of Their Novel Application in Statistical Mechanics

The foundation of random matrices theory can be traced back to its inception within the realm of nuclear physics, as E. Wigner [4,5] pioneered its development to describe the intricate energy levels of heavy nuclei. Wigner achieved this by representing the nucleus's Hamiltonian using matrices with randomly distributed entries.

When considering symmetric matrices ($h_{ij} = h_{ji}$) with well-behaved entries, i.e., entries following a probability density function $f(h)$ such that

$$\int_{-\infty}^{\infty} dh_{ij} f(h_{ij}) h_{ij} < \infty, \tag{4}$$

$$\int_{-\infty}^{\infty} dh_{ij} f(h_{ij}) h_{ij}^2 < \infty$$

of a matrix H , with dimensions $N \times N$, featuring independent entries, and thus, characterized by a joint distribution given as:

$$\begin{aligned} \Pr(h_{11}, h_{12}, \dots, h_{NN}) &= \Pr(\{h_{ij}\}_{i \leq j}) \\ &= \prod_{i < j} f(h_{ij}). \end{aligned} \tag{5}$$

This leads to a joint eigenvalue distribution $P(\lambda_1, \dots, \lambda_N)$, and its eigenvalue density is defined as follows:

$$\sigma(\lambda) = \int_{-\infty}^{\infty} \dots \int_{-\infty}^{\infty} P(\lambda, \lambda_2, \lambda_3, \dots, \lambda_N) d\lambda_2 d\lambda_3 \dots d\lambda_N, \tag{6}$$

which, under the earlier-stated conditions for the matrix entries h_{ji} , is universally characterized by the semi-circle law [13,14]:

$$\sigma(\lambda) = \begin{cases} \frac{1}{\pi} \sqrt{2N - \lambda^2} & \text{if } \lambda^2 < 2N \\ 0 & \text{if } \lambda^2 \geq 2N \end{cases} \tag{7}$$

In the particular context where $f(h_{ij}) = \frac{e^{-h_{ij}^2/2}}{\sqrt{2\pi}}$, we can establish the Boltzmann weight as follows:

$$P(\lambda_1, \dots, \lambda_N) = C_N \exp \left[-\frac{1}{2} \sum_{i=1}^N \lambda_i^2 + \sum_{i < j} \ln |\lambda_i - \lambda_j| \right],$$

where $C_N^{-1} = \int_0^{\infty} \dots \int_0^{\infty} d\lambda_1 \dots d\lambda_N \exp[-\mathcal{H}(\lambda_1 \dots \lambda_N)]$ denotes the inverse of the normalization constant for a Coulomb gas with the Hamiltonian:

$$\mathcal{H}(\lambda_1 \dots \lambda_N) = \frac{1}{2} \sum_{i=1}^N \lambda_i^2 - \sum_{i < j} \ln |\lambda_i - \lambda_j|$$

operating at an inverse temperature $\beta^{-1} = 1$. The final term exhibits logarithmic repulsion, akin to the conventional Wigner/Dyson ensembles, as elucidated by Dyson [6]. Simultaneously, the first term exerts an attractive influence. In the context of Hermitian or symplectic entries, as elucidated by Mehta [13], the outcome remains comparable. Specifically, it yields $P(\lambda_1, \dots, \lambda_N) = C_N^\beta \exp(-\beta \mathcal{H})$, with β taking values of 2 and 4, resulting in a consistently shared eigenvalue density (7).

Despite the apparent analogy, there is no immediate bridge between the thermodynamics of a real-world system and the fluctuations observed in random matrices generated from data originating from that very system. However, when one delves deeper into the quest for correlations, this bridge starts to materialize. Its comprehension holds the key to unlocking insights into phase transitions and critical phenomena within thermostatics.

It is worth noting that, nearly three decades before Wigner and Dyson’s groundbreaking work, Wishart [7] pioneered the analysis of correlated time series. Rather than resorting to Gaussian or unitary ensembles, he delved into the realm of the Wishart ensemble. This

ensemble primarily deals with random correlation matrices, distinguishing it from the conventional approaches of his contemporaries.

In recent contributions [8], we explored this avenue by introducing the magnetization matrix element m_{ij} representing the magnetization of the j th time series at the i th Monte Carlo (MC) step within a system of $N = L^d$ spins. For simplicity in our investigations, we adopted $d = 2$, the minimum dimension where a phase transition occurs in the simple Ising model. Additionally, we delved into the mean-field Ising model [9], maintaining the same total number of spins.

Here, $i = 1, \dots, N_{MC}$, and $j = 1, \dots, N_{sample}$. Consequently, the magnetization matrix M assumes dimensions $N_{MC} \times N_{sample}$. To scrutinize the spectral properties more effectively, we propose an intriguing alternative: rather than analyzing M , we turn our attention to the square matrix of dimensions $N_{sample} \times N_{sample}$:

$$G = \frac{1}{N_{MC}} M^T M,$$

resulting in $G_{ij} = \frac{1}{N_{MC}} \sum_{k=1}^{N_{MC}} m_{ki} m_{kj}$, a matrix well-known as the Wishart matrix [7]. At this juncture, rather than continuing with m_{ij} , it becomes more advantageous to operate with the matrix M^* , whose elements are defined through the customary variables:

$$m_{ij}^* = \frac{m_{ij} - \langle m_j \rangle}{\sqrt{\langle m_j^2 \rangle - \langle m_j \rangle^2}},$$

where:

$$\langle m_j^k \rangle = \frac{1}{N_{MC}} \sum_{i=1}^{N_{MC}} m_{ij}^k.$$

Thereby:

$$\begin{aligned} G_{ij}^* &= \frac{1}{N_{MC}} \sum_{k=1}^{N_{MC}} \frac{m_{ki} - \langle m_i \rangle}{\sqrt{\langle m_i^2 \rangle - \langle m_i \rangle^2}} \frac{m_{kj} - \langle m_j \rangle}{\sqrt{\langle m_j^2 \rangle - \langle m_j \rangle^2}} \\ &= \frac{\langle m_i m_j \rangle - \langle m_i \rangle \langle m_j \rangle}{\sigma_i \sigma_j} \end{aligned} \tag{8}$$

where $\langle m_i m_j \rangle = \frac{1}{N_{MC}} \sum_{k=1}^{N_{MC}} m_{ki} m_{kj}$ and $\sigma_i = \sqrt{\langle m_i^2 \rangle - \langle m_i \rangle^2}$. Analytically, when m_{ij}^* are uncorrelated random variables, the joint distribution of eigenvalues can be described by the Boltzmann weight [15,16]:

$$\begin{aligned} P(\lambda_1, \dots, \lambda_{N_{sample}}) &= C_{N_{sample}} \exp \left[-\frac{N_{MC}}{2} \sum_{i=1}^{N_{sample}} \lambda_i + \frac{(N_{MC} - N_{sample} - 1)}{2} \sum_{i=1}^{N_{sample}} \ln \lambda_i \right. \\ &\quad \left. + \sum_{i < j} \ln |\lambda_i - \lambda_j| \right] \end{aligned}$$

where $C_{N_{sample}}^{-1} = \int_0^\infty \dots \int_0^\infty d\lambda_1 \dots d\lambda_{N_{sample}} \exp[-\mathcal{H}(\lambda_1 \dots \lambda_{N_{sample}})]$, and this corresponds to the Hamiltonian:

$$\mathcal{H}(\lambda_1 \dots \lambda_{N_{sample}}) = \frac{N_{MC}}{2} \sum_{i=1}^{N_{sample}} \lambda_i - \frac{(N_{MC} - N_{sample} - 1)}{2} \sum_{i=1}^{N_{sample}} \ln \lambda_i - \sum_{i < j} \ln |\lambda_i - \lambda_j|.$$

In this case, the density of eigenvalues $\rho(\lambda)$ of the matrix $G^* = \frac{1}{N_{MC}} M^{*T} M^*$ follows the well-known Marchenko–Pastur distribution or Marchenko–Pastur (MP) law [10], which, for our case, we write as:

$$\rho(\lambda) = \begin{cases} \frac{N_{MC}}{2\pi N_{sample}} \frac{\sqrt{(\lambda - \lambda_-)(\lambda_+ - \lambda)}}{\lambda} & \text{if } \lambda_- \leq \lambda \leq \lambda_+ \\ 0 & \text{otherwise,} \end{cases} \tag{9}$$

where $\lambda_{\pm} = 1 + \frac{N_{sample}}{N_{MC}} \pm 2\sqrt{\frac{N_{sample}}{N_{MC}}}$.

In our studies [8,9], we examined the behavior of $\rho_{numerical}(\lambda)$ by analyzing the m_{ij} data obtained from both a two-dimensional Ising model and a mean-field Ising model. These models were simulated at various temperatures using the single-spin flip Metropolis dynamics.

In the first scenario, we considered square lattices with a linear dimension $L = 100$, resulting in a total of $N = 10,000$ spins. We maintained the same number of spins in the second case. Our simulations employed $N_{MC} = 300$ and $N_{sample} = 100$, which is computationally highly efficient.

We repeated the process $N_{run} = 1000$ times to generate a sufficient number of eigenvalues for constructing histograms and calculating numerical moments:

$$\langle \lambda^k \rangle_{numerical} = \frac{\sum_{i=1}^{N_{bins}} \lambda_i^k \rho_{numerical}(\lambda_i)}{\sum_{i=1}^{N_{bins}} \rho_{numerical}(\lambda_i)}, \tag{10}$$

Our histograms were constructed with $N_{bins} = 100$. We anticipate that $\rho_{numerical}(\lambda)$ should approach $\rho(\lambda)$ according to Equation (9) as $T \rightarrow \infty$ (in the paramagnetic phase). In this situation, $\langle \lambda^k \rangle_{numerical}$ should closely align with the theoretical value:

$$\langle \lambda^k \rangle = \int_{-\infty}^{\infty} \lambda^k \rho(\lambda) d\lambda = \sum_{j=0}^{k-1} \frac{\left(\frac{N_{sample}}{N_{MC}}\right)^j}{j+1} \binom{k}{j} \binom{k-1}{j}. \tag{11}$$

where this relation is deduced by expanding the binomials and utilizing the well-known Vandermonde identity: $\sum_{l=0}^r \binom{m}{l} \binom{n}{r-l} = \binom{m+n}{r}$. For $k = 1$, $\langle \lambda \rangle = 1$, and we expect $\langle \lambda \rangle_{numerical} \approx 1$ as $T \rightarrow \infty$. On the other hand, the second moment:

$$\langle \lambda^2 \rangle = \sum_{j=0}^1 \frac{\left(\frac{N_{sample}}{N_{MC}}\right)^j}{j+1} \binom{2}{j} \binom{1}{j} = 1 + \left(\frac{N_{sample}}{N_{MC}}\right).$$

Hence, we find that $\langle \lambda^2 \rangle - \langle \lambda \rangle^2$ equals $\frac{N_{sample}}{N_{MC}}$. In our current scenario, $\langle \lambda^2 \rangle - \langle \lambda \rangle^2$ equals $\frac{1}{3}$, and we, therefore, anticipate this value numerically as T approaches infinity.

However, for $T \approx T_C$ or $T < T_C$, the results warrant closer examination. We are now presenting, as a revised version, the results regarding fluctuations in the Ising model, both in the two-dimensional and mean-field approximations, as functions of temperature, employing the parameters described above, as detailed in [8,9]. Figure 1 vividly illustrates that fluctuations exhibit a distinctive response concerning critical phenomena in the Ising model. This phenomenon holds true irrespective of whether we are considering Monte Carlo simulations in the two-dimensional Ising model or its mean-field approximation.

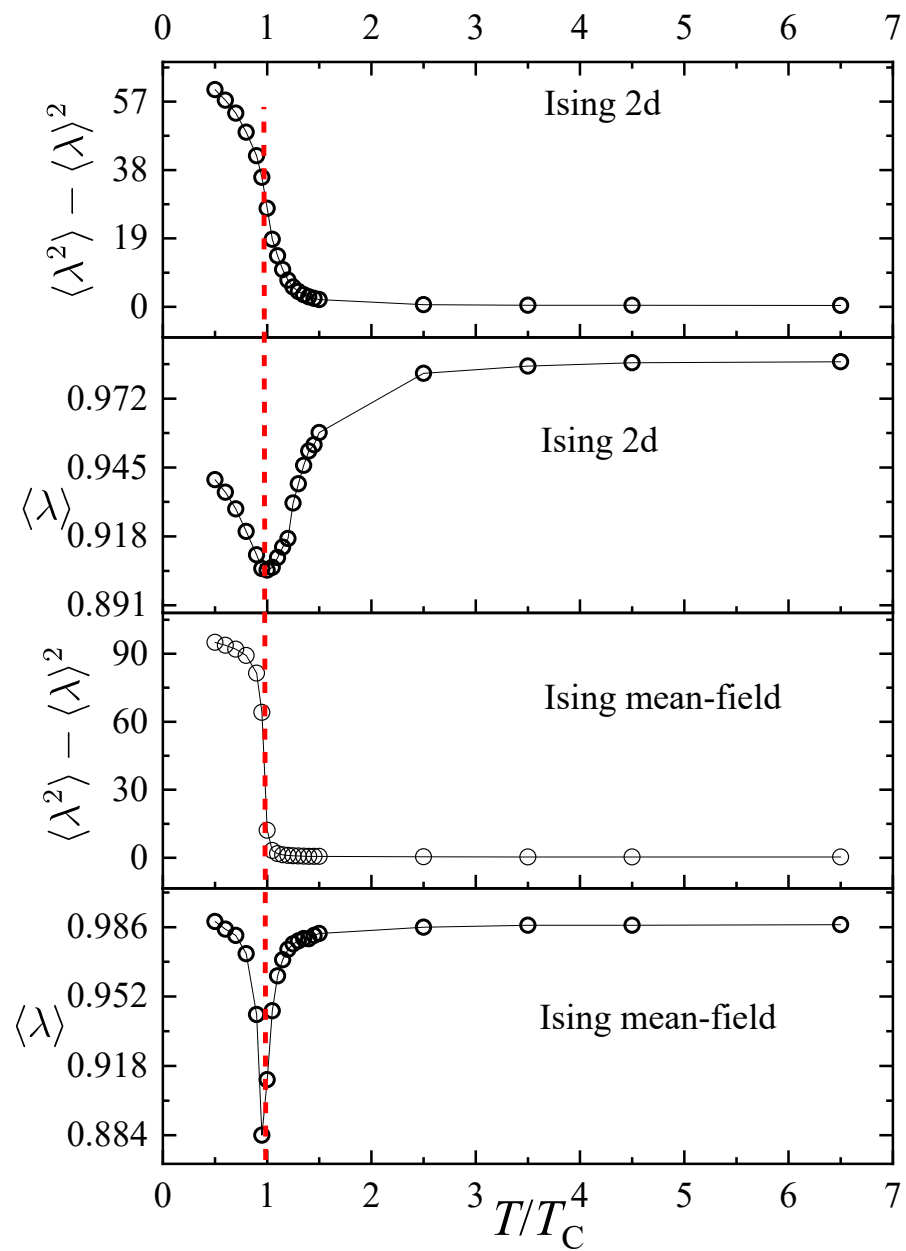


Figure 1. The fluctuations of eigenvalues in G were examined, taking into account the Ising model in two settings: a two-dimensional square lattice and a mean-field approximation, as reported in [8,9]. Notably, we can discern a distinct peak occurring at $T = T_C$ for the average eigenvalue in both formulations of the Ising model. Additionally, an inflection point becomes apparent in the variance of the eigenvalue.

We can clearly discern a minimum point in the behavior of $\langle \lambda \rangle$ and an inflection point in $\langle \lambda^2 \rangle - \langle \lambda \rangle^2$ occurring precisely at $T = T_C$. As discussed in detail in [8,9], this phenomenon is closely tied to the emergence of a gap when $T < T_C$, which subsequently closes as T approaches T_C . For a more-comprehensive understanding, please refer to [8,9]. It is worth noting that $\langle \lambda \rangle_{\text{numerical}}$ approximates to 1 for large values of T .

However, an intriguing question arises: How do $\langle \lambda \rangle$ and $\langle \lambda^2 \rangle - \langle \lambda \rangle^2$ behave when considering iterations of the Chirikov map instead of time series data from spin systems? In the following section, we present the key findings of this study.

3. Main Results

We conducted iterations of the Chirikov map, mirroring the approach employed in our study of the Ising model. In this case, we obtained matrix elements m_{ij} , which can now represent q_{ij} (iterations for position coordinates) or p_{ij} (iterations for moments). Here, $i = 1, \dots, N_{MC} = 200$ iteration steps (It is worth noting that, in keeping with our established notation convention, we employed N_{MC} to denote the number of map iterations. The abbreviation MC is derived from our previous example involving Monte Carlo simulations for the Ising model,) and j ranges from 1 to $N_{sample} = 100$ different series. To initiate this process, we initialized random values for q_0 within the range $[0, 2\pi]$ and p_0 within the range $[0, 2\pi]$.

To provide a pedagogical visualization of the map iteration, let us consider a simple example. We observed the time evolutions q_i and p_i as functions of step $i = 1, 2, \dots, 100$. For a clearer visualization, consider focusing on the initial 100 steps, for three different initial conditions: $j = 1$ ($p_0 = 0.1$ and $q_0 = \pi$), $j = 2$ ($p_0 = 1$ and $q_0 = 1$), and $j = 3$ ($p_0 = \pi$ and $q_0 = 0.1$). These evolutions are presented in Figure 2, with the sequences displayed from bottom to top.

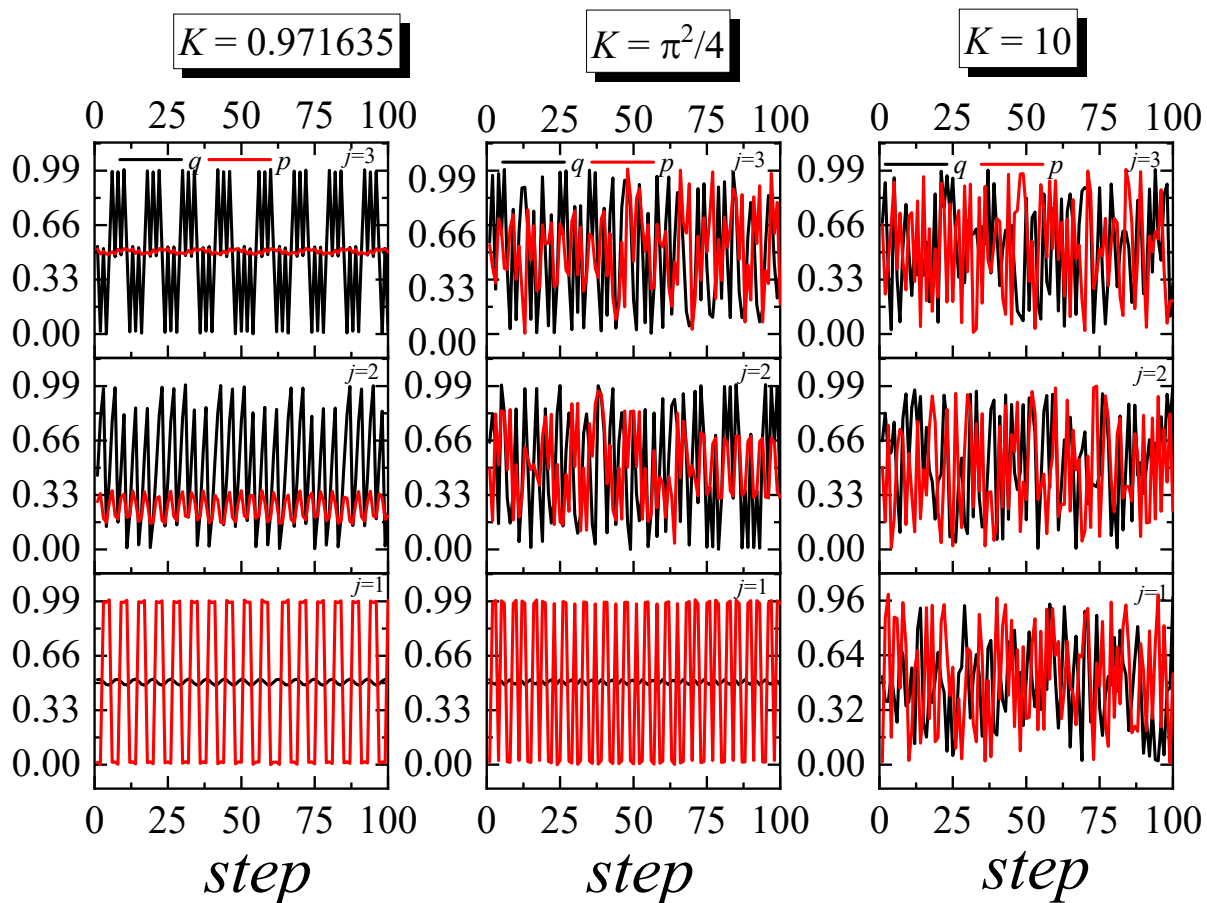


Figure 2. We engaged in iterations of moment and position coordinates within the framework of Chirikov's map. The columns of matrix M were populated with N_{sample} iterations of position and moment pairs q_{ij} , p_{ij} . To illustrate this, we present a sample of time evolutions originating from three distinct initial conditions $(p_0, q_0) = (0.1, \pi)$, $(1, \pi)$, and $(\pi, 0.1)$, respectively, displayed from bottom to top. These evolutions were examined under three different parameter values: $K = 0.971635$ (signifying the destruction of the golden KAM curve), $\frac{\pi^2}{4}$ (corresponding to the Chirikov criteria for the chaos border), and 10 (indicative of a state of complete chaos).

For the sake of illustration, we selected three distinct values of K . The first, $K = 0.971635$, signifies a scenario where the golden KAM curve is theoretically destroyed. The second,

$K = \frac{\pi^2}{4}$, aligns with the Chirikov resonance overlap criterion for defining the chaos border. Lastly, we considered $K = 10$, representing a situation characterized by complete and unbridled chaos.

To enhance the illustrative aspect, we also generated Poincaré sections corresponding to these three parameters, primarily for pedagogical purposes. To create these sections, we explored values for $(N_p + 1)(N_q + 1)$ different initial conditions parametrized as follows: $q_0 = \frac{2\pi}{N_q}l_q$ and $p_0 = \frac{2\pi}{N_p}l_p$, where $l_q = 0, 1, \dots, N_q$ and $l_p = 0, 1, \dots, N_p$. For an effective visualization, we employed $N_q = N_p = 20$, resulting in q_0 and p_0 residing within the range $[0, 2\pi]$.

The intriguing and anticipated patterns can be vividly appreciated in Figure 3. Following this pedagogical exploration of the Chirikov method, we now proceed to utilize the random matrix method proposed here to shed light on the chaos border.

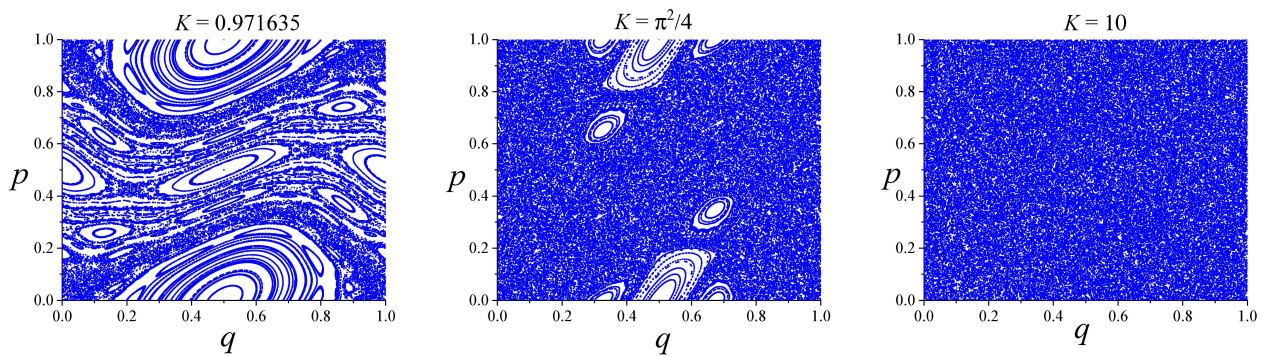


Figure 3. Poincaré sections were constructed for the same set of K values employed in Figure 2.

Our algorithm constructs an ensemble of matrices, comprising $N_{run} = 1000$ distinct matrices G^* of dimension $N_{sample} \times N_{sample}$. These matrices correspond to N_{run} varying initial conditions, which are randomly selected with $q_0, p_0 \in [0, 2\pi]$. Subsequently, we diagonalized these matrices and organized the eigenvalues within the interval $\lambda_{min}^{(Numerical)}$ to $\lambda_{max}^{(Numerical)}$. We maintained a fixed number of bins, $N_{bin} = 100$, and generated histograms to calculate $\rho_{numerical}(\lambda_i)$.

We carried out this process for various values of K , ranging from $K_{min} = 0$ to $K_{max} = 10$. Consequently, we present the numerical density of the eigenvalues for three distinct K values in Figure 4. In this figure, we present the eigenvalues of G^* obtained from the time evolutions of q and p , whose components are given, respectively, by:

$$G_{ij}^{(q)*} = \frac{\langle q_i q_j \rangle - \langle q_i \rangle \langle q_j \rangle}{\sigma_i^{(q)} \sigma_j^{(q)}} \text{ and } G_{ij}^{(p)*} = \frac{\langle p_i p_j \rangle - \langle p_i \rangle \langle p_j \rangle}{\sigma_i^{(p)} \sigma_j^{(p)}},$$

where the terms $\langle x_i \rangle$ are calculated as the mean values $\langle x_i \rangle = \frac{1}{N_{MC}} \sum_{k=1}^{N_{MC}} x_{ki}$ and $\langle x_i x_j \rangle$ as the covariance, given by $\langle x_i x_j \rangle = \frac{1}{N_{MC}} \sum_{k=1}^{N_{MC}} x_{ki} x_{kj}$. The standard deviations, $\sigma_i^{(x)}$, are computed as $\sigma_i^{(x)} = \sqrt{\langle x_i^2 \rangle - \langle x_i \rangle^2}$, where x can be either q or p .

It is noteworthy that, for small values of K , a noticeable difference is observed when compared to the MP law density, as described by Equation (9). However, for $K = 10$, a substantial match between the numerical results and the theoretical prediction (MP law; see Equation (9)) is evident. It is important to note that this match is not perfect, which aligns with the expectations since a perfect match would typically occur only for entirely random time series, not those displaying complete chaos.

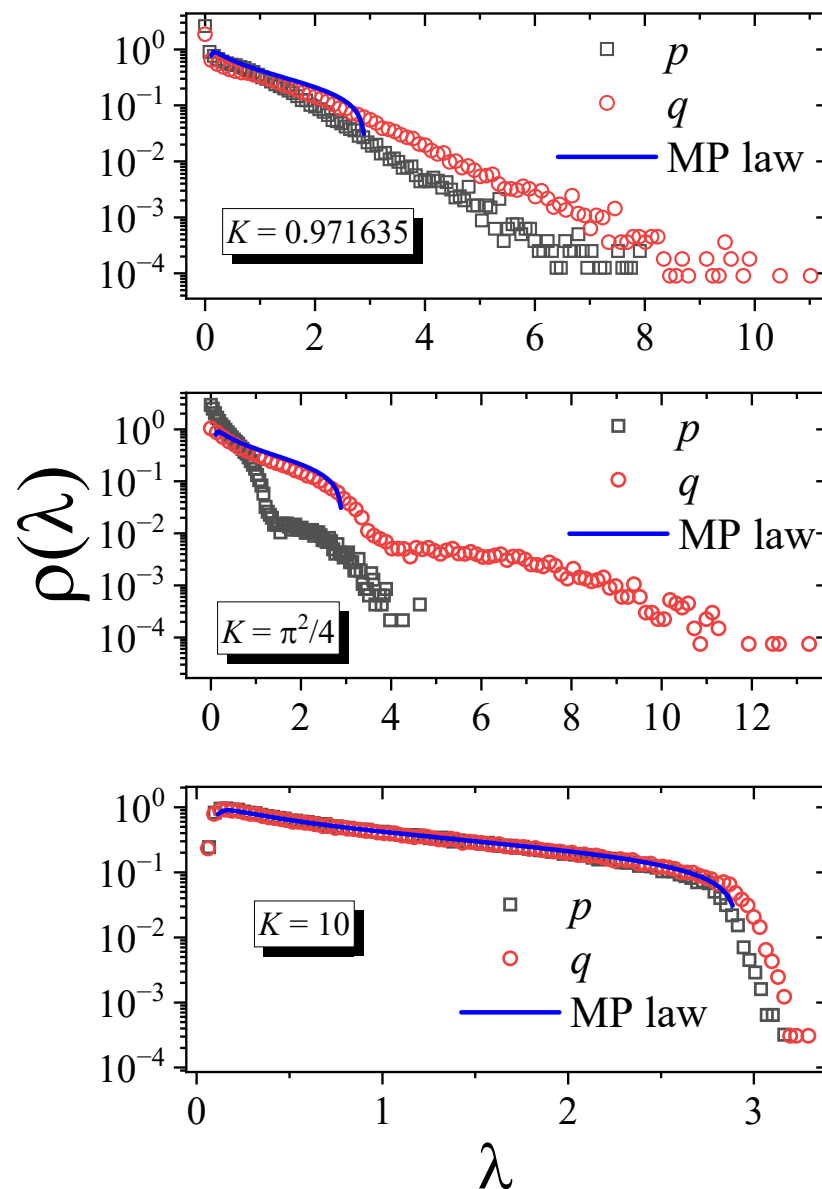


Figure 4. The density of eigenvalues for various K values is depicted here. In the chaotic regime, we can discern a notable alignment with the MP law, indicating a good fit.

This hints at a potential approach to distinguish chaos from random behavior, a pivotal point emphasized in [17]. Our exploration in this direction shows promise in addressing this challenge, as suggested by preliminary observations in material currently under preparation. This underscores the importance of sustained focus in our future research endeavors.

In the context of spin systems (as discussed in [8,9]), we observed a restoration of the Marchenko–Pastur law at elevated temperatures. While the system is predominantly stochastic rather than highly chaotic in this scenario, we can draw a meaningful analogy. To further investigate this phenomenon, we examine the fluctuations of eigenvalues, as described in Equation (10), particularly those derived from the time evolutions of moments.

These results are visually depicted in Figure 5. It is quite intriguing to decipher the insights conveyed by this plot. In Figure 5a, the fluctuations in the average eigenvalue are displayed as a function of K for 10 different seeds. Notably, the outcomes exhibit minimal variation across different seeds. Figure 5b presents the same plot along with error bars for added clarity.

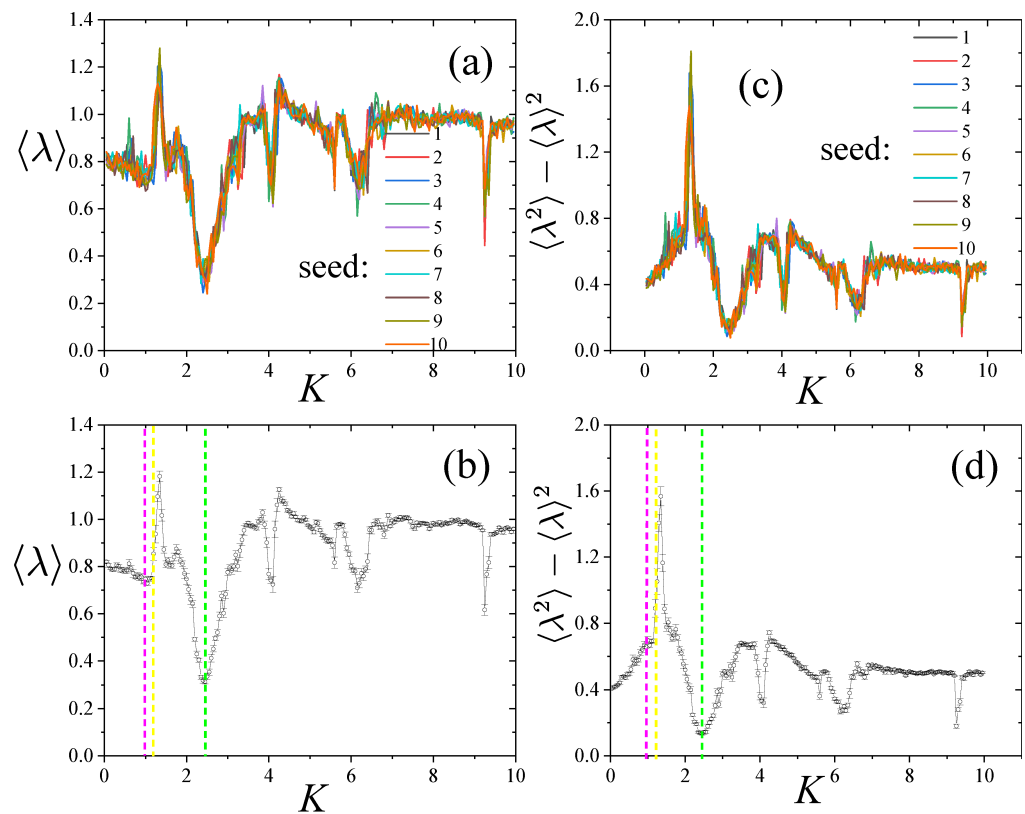


Figure 5. The exploration of fluctuations in the eigenvalues of matrix G^* entails constructing it based on the time evolutions of p . Figures (a) and (c) portray the average and variance, respectively, across 10 different seeds of the simulation. Meanwhile, Figures (b) and (d) illustrate the mean values of these respective quantities, averaged over the same set of different seeds used to obtain the error bars.

We observed that the global minimum, denoted by the green dashed line, precisely occurs at $K \approx 2.46$, not by coincidence. This numerical value aligns with $\pi^2/4$, which corresponds to the Chirikov resonance overlap criterion for the border of chaos. This same pattern emerges in the dispersion of eigenvalues, as depicted in both Figure 5c,d. The former illustrates the variance among different seeds, while the latter shows the average under these seeds. Remarkably, $K \approx 2.46$ also serves as the global minimum for the dispersion of eigenvalues.

The value $K \approx 2.46$ is greater than $K = 0.9716$ for several reasons, notably due to the influence of secondary-order resonances and the finite width of the chaotic layer. An intriguing study by Frahm and Shepelyansky [18] delved into what they referred to as the “Chirikov typical map” a modification of the well-known Chirikov standard map, which introduced a finite number of random phase shift angles originally also proposed by B. Chirikov [11]. Their findings suggest that the effects observed in the Chirikov typical map are comparatively less pronounced than those seen in the original version (standard map).

Furthermore, it is worth noting that $K = 0.9716$, indicated by the dashed magenta line in the same plot, anticipates a significant upturn in both behaviors, specifically in $\langle \lambda \rangle \times K$ and $\langle \lambda^2 \rangle - \langle \lambda \rangle^2 \times K$. This trend seems to exhibit universality. Lichtenberg and Lieberman [1] proposed a refinement of K as $K = \frac{\pi^2}{4}$, which would suggest $K \approx 1.2$. This refinement is represented by the yellow dashed line in Figure 5. It is evident that this point consistently demonstrates an increase after the critical $K = 0.9716$.

To provide a comprehensive view, we also examined the eigenvalues associated with the time evolutions of positions. Interestingly, we continued to observe the global minimum occurring at approximately $K \approx 2.46$, aligning with the Chirikov resonance overlap criterion for the chaos boundary. This pattern appears to exhibit universality. However, a noteworthy departure arises when considering the eigenvalue dispersion,

as we now observe a global maximum at the same K value. This intriguing phenomenon is depicted in Figure 6. To maintain consistency, we employed a similar approach to illustrate the points $K = 0.9716$ and $K \approx 1.2$.

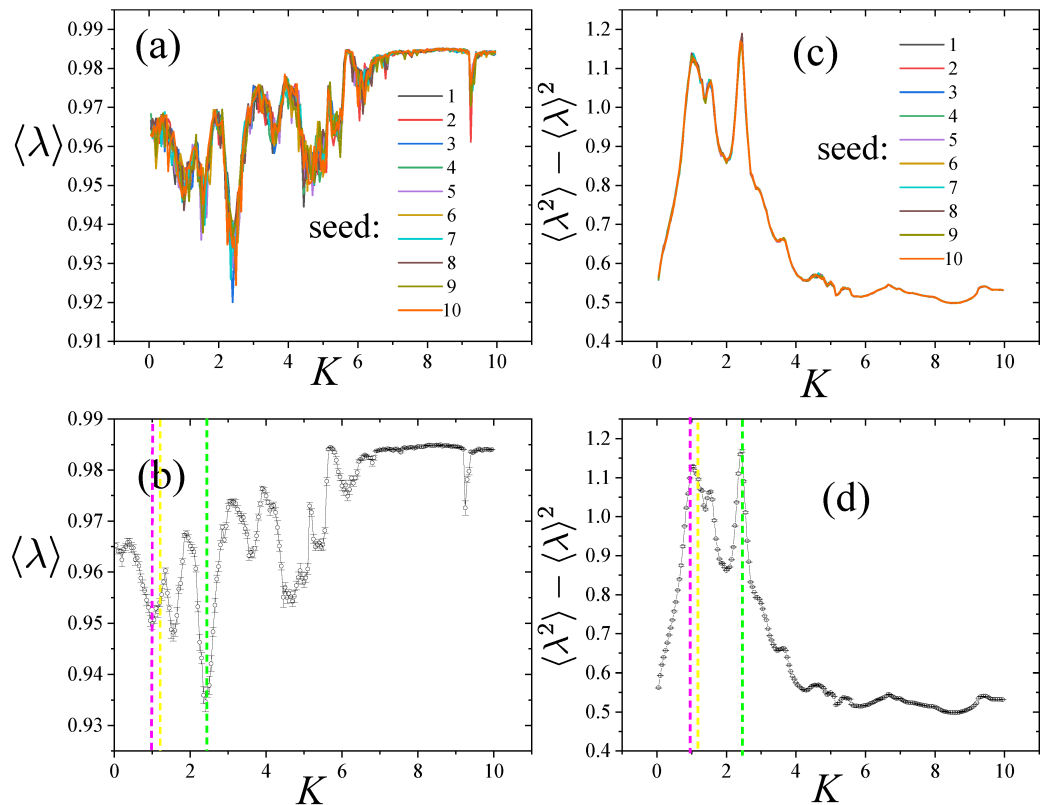


Figure 6. Examining eigenvalue fluctuations in the matrix G^* constructed through iterations of q (various time evolutions). (a,c) display the average and variance across 10 simulation seeds, while (b,d) demonstrate the mean values of these quantities, averaged over the same set of seeds—used in this instance for error bar derivation.

4. Examining the Approach in a Different Map and Contrasting It with Alternative Techniques

What do alternative techniques reveal about our method? To explore this, we were inspired by a technique used, for example, in [19,20]. This technique enables us to decipher the bifurcation diagram in conservative systems. It involves plotting the Lyapunov exponent corresponding to each q_0 across varying parameter values of K . In essence, our iteration for the positional coordinate can be expressed as follows:

$$q_{n+1} = f(q_n, p_n) = q_n + p_n + K \sin q_n$$

As we iterate the map starting from q_0 , focusing solely on constructing the Lyapunov exponent based on positional coordinates, as this suffices for our analysis, we generated a sequence of iterations, q_0, q_1 , and so on, up to $q_{N_{MC}-1}$. The calculation of the Lyapunov exponent is as follows:

$$\lambda(q_0, K) = \frac{1}{N_{MC}} \sum_{j=0}^{N_{MC}-1} \ln \left| \frac{\partial f(q_j, p_j)}{\partial p_j} \right|$$

For the sake of simplicity, we set $p_0 = 0$ in Chirikov’s map iteration. Therefore:

$$\lambda(q_0, K) = \frac{1}{N_{MC}} \sum_{j=0}^{N_{MC}-1} \ln|1 + K \cos q_j| = \frac{1}{N_{MC}} \ln \left(\prod_{j=0}^{N_{MC}-1} |1 + K \cos q_j| \right).$$

For each pair (q_0, K) , we derived $\lambda(q_0, K)$. Our variation of q_0 spanned the interval $[0, 2\pi]$, while K ranged within $[0, 4]$. The results are presented in the form of a color diagram shown in Figure 7.

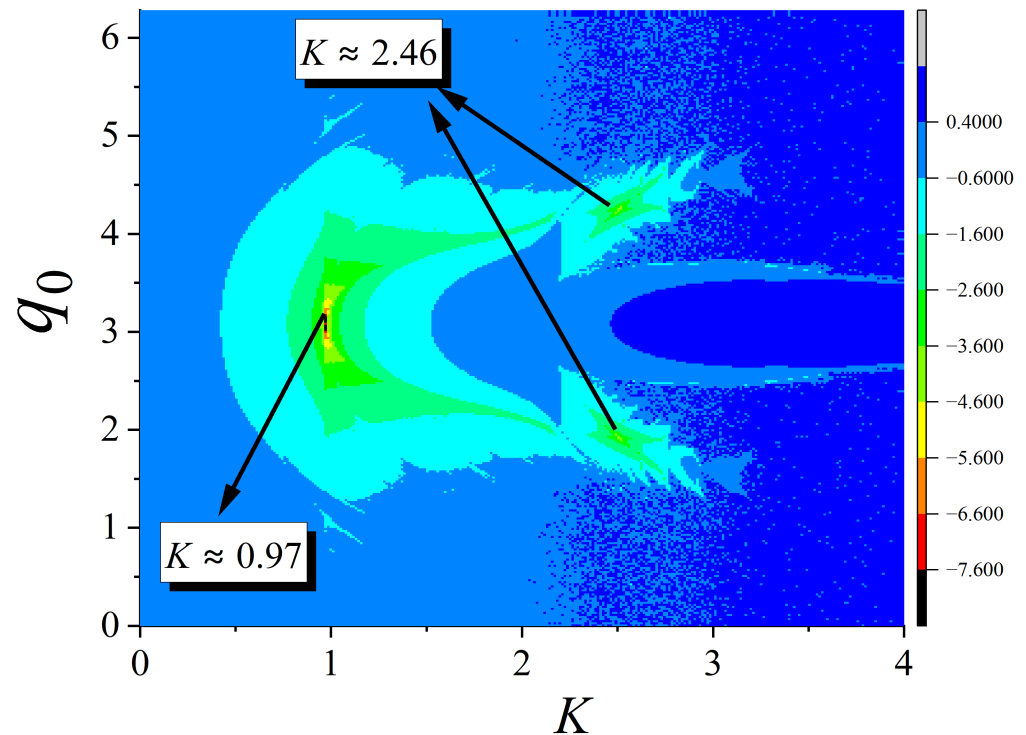


Figure 7. Liapunov exponent in the mixed space phase $q_0 \times K$ for the standard map with $p_0 = 0$. Utilizing a grid of 300×300 points and $n = 500$ iterations.

We can visualize the Lyapunov exponent in the mixed phase space $(q_0 \times K)$ for the standard map, with the condition $p_0 = 0$. Our approach involved a grid comprising 300×300 points and a total of $N_{MC} = 500$ iterations of the map. Let us focus our attention on points exhibiting higher Lyapunov exponents. To do so, it is crucial to note that two minuscule yellow regions, symmetrically situated with respect to $q = \pi$, are observed within two equally symmetric green regions. These correspond precisely to $K \approx 2.46$. Similarly, a very small red region can be discerned at $K \approx 0.97$, as indicated by the arrows in Figure 7. Consequently, these observations, respectively, align with the Chirikov resonance overlap criterion for the chaos boundary and the transition parameter where the golden KAM curve is theoretically disrupted, corroborating our random matrix method’s findings.

However, one crucial point warrants further exploration: Is our random matrix method efficient for studying other models? To address this, we chose to investigate the one-dimensional logistic map, a paradigmatic and extensively explored example of a chaotic system:

$$x_{n+1} = r x_n (1 - x_n),$$

where the parameter r falls within the range: $0 < r < 4$. When we iteratively apply this unimodal map: $x_1 = rx_0(1 - x_0)$, $x_2 = rx_1(1 - x_1)$, and so forth, it is essential to note that $0 \leq x_n \leq 1$, ensuring that $x_0 \in [0, 1]$.

It is well documented that, for $r > 3$, the onset of a cascading bifurcation sequence occurs, as depicted in Figure 8a. This cascade persists from approximately $r \approx 3.57$, concluding abruptly at $r = 4$, precisely within the chaotic region of this map.

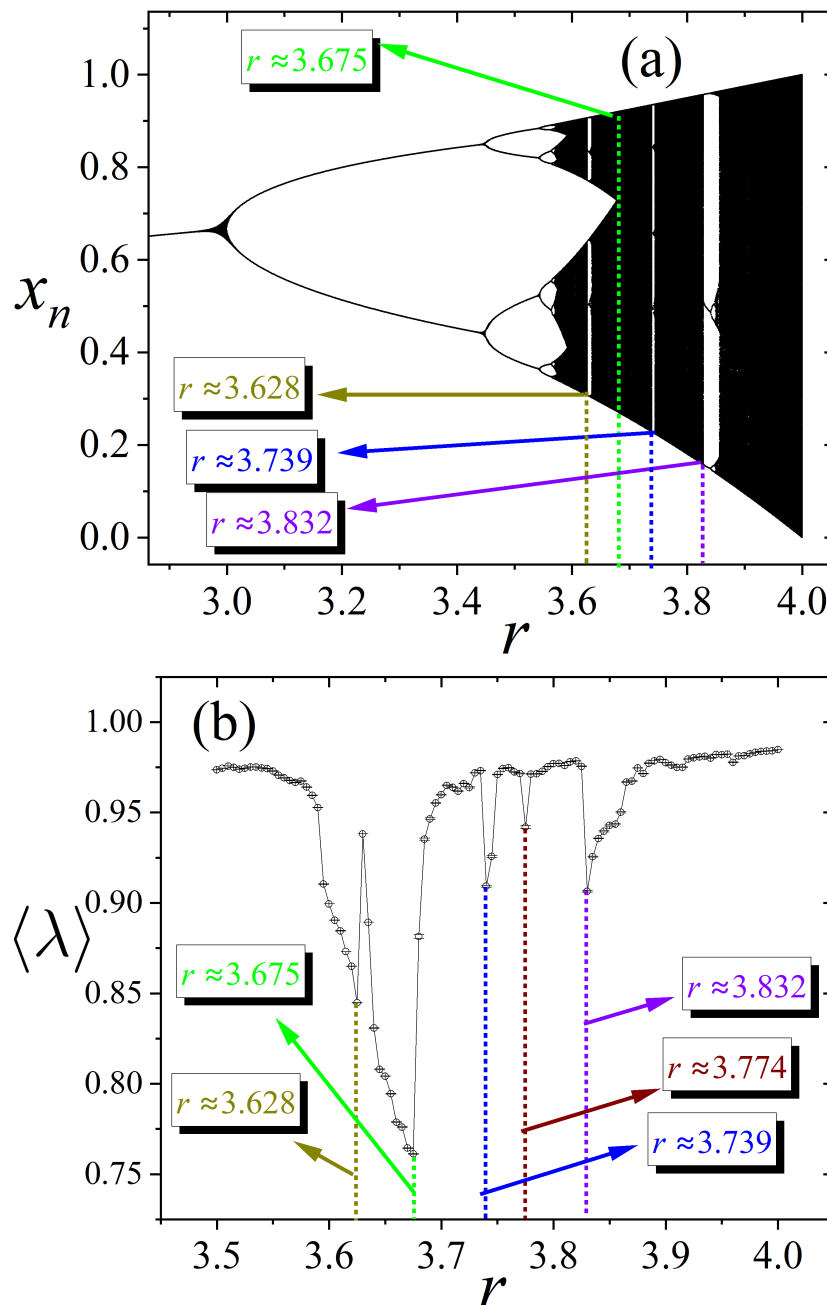


Figure 8. (a) The bifurcation diagram of the logistic map, highlighting crucial parameters for further exploration in (b) below. (b) A plot depicting the average eigenvalue of a Wishart matrix derived from the dynamic evolution of the logistic map, demonstrating its dependence on the parameter r .

We conducted an identical study to the one previously performed on the Chirikov map, this time focusing on the logistic map. The process involved iterating the system for $N_{sample} = 100$ different time series of x_n , with $n = 1, 2, \dots, N_{MC} = 200$ iterations, to construct a matrix G (with dimensions $N_{sample} \times N_{sample}$) and compute its eigenvalues. Similar to our previous approach, we generated $N_{run} = 1000$ distinct matrices G , each associated with a randomly chosen initial condition, x_0 , from the interval $[0, 1]$. This yielded a total of 10^5 eigenvalues to ensure robust statistical analysis.

We obtained the eigenvalue distribution and calculated the average eigenvalue by plotting $\langle \lambda \rangle$ as a function of r , mirroring the approach we used for the Chirikov standard map. The corresponding results can be found in Figure 8b.

It is crucial to identify specific points that correspond to significant structural features in the bifurcation diagram of the logistic map, as depicted in Figure 8a, and then, compare them with the insights presented in Figure 8b. Notably, in Figure 8b, the average eigenvalue exhibits a distinctive global minimum (indicated by the green line) around $r \approx 3.675$.

What is particularly intriguing is that this specific r -value aligns with the region that predominantly represents chaotic behavior in the bifurcation diagram of the logistic map, as depicted in Figure 8a. Notably, this value precisely coincides with the point marking the tip of the pointed chaotic region, slightly exceeding $r \approx 3.57$. It is here that the cascade of bifurcations of the period accumulates, in accordance with the predictions of Feigenbaum [21].

However, it is noteworthy that the other minima correspond to the visually blank stripes in the logistic map. It is truly remarkable that our proposed spectral method in this study exhibited such strong correspondence with these regions. Yet, there was one exception: at $r \approx 3.774$, there is no blank region in the logistic map for this minimum. This anomaly underscores the limitations of relying solely on visualizations of the logistic map, and it calls for a thorough investigation of this specific point.

The explanation for this can be traced back to the insightful work of Metropolis et al. in 1973 [22]. In the specific case of unimodal maps, like the logistic map, there is a single critical point ($x_c = 1/2$ in this context), and superstable orbits of period $m = 1, 2, 3, \dots$, necessarily include this critical point. These authors conducted a thorough investigation into the ordering of such orbits as the parameter r undergoes variations. Consequently, for the logistic map, $x_c = 1/2$ consistently serves as a member of any superstable m -cycle, while the other points of the cycle are denoted by the labels “R” and “L”, with the understanding that $x_n \rightarrow R$ when $x_n > 1/2$ and $x_n \rightarrow L$ when $x_n < 1/2$.

In total, there are 20 universal sequences at our disposal. To illustrate, if we commence with $x_0 = 1/2$ and progress to $x_1 > 1/2$, subsequently shifting to $x_2 < 1/2$ before returning to $x_0 = 1/2$, we establish a superstable three-cycle of the RL variety. This particular scenario materializes at $r = 3.8318741$. To streamline our analysis, we extracted the r -values of interest from [22], which are presented in Table 1. This table delineates the universal sequences that manifest under various conditions.

Table 1. Key universal sequences pertinent to the logistic map in this study. Extracted from reference [22].

Period	Sequence	r
6	RLRRR	3.6275575
5	RLRR	3.7389149
7	RLRRLR	3.7742142
3	RL	3.8318741

It is noteworthy that all the minimum values identified through our method precisely align with the r -values predicted in [22]. For instance, the minimum we discovered at $r \approx 3.774$ corresponds to a seven-cycle, a phenomenon that was not visually discernible in the bifurcation diagram. This underscores the efficacy of our method, which adeptly captures the intricate subtleties of the logistic map, much like it did in our previous analysis of the Chirikov’s standard map.

5. Conclusions

In our study, we utilized the technique of Wishart-like matrix spectra fluctuations to probe the existence of chaos within Chirikov’s standard map. This methodology drew inspiration from its past success in characterizing critical points within spin systems. Our

results consistently affirmed that the resonance overlap criterion for the chaos boundary, denoted as $K = \left(\frac{\pi}{4}\right)^2 \approx 2.46$, holds true whether we examine the spectra obtained from the evolutions of moments or from the evolutions of position coordinates.

However, intriguingly, when it comes to the dispersion, $\langle \lambda^2 \rangle - \langle \lambda \rangle^2$, this same K value remained a global minimum for the evolutions of moments, but transformed into a global maximum for the evolutions of positions.

Furthermore, the value $K = 0.971635$, which marks the point at which the golden KAM curve is disrupted, appeared to foreshadow extreme behaviors in the eigenvalue fluctuations. The outcomes of our method were further validated using conventional techniques that combined Lyapunov exponent analysis with bifurcation diagram schemes.

This study holds promise in unraveling the intricate relationship between chaos and quantum mechanics, but it merits further exploration and extension to other models. Such analyses could prove invaluable in enhancing our understanding of this complex interplay.

In addition, to evaluate the method's robustness, we applied it to analyze the logistic map. Our method confirmed the presence of superstable cycles of varying orders across different parameter settings, a confirmation supported by the corresponding bifurcation diagrams. We firmly believe that our methodology should be extended to continuous maps, as it allows for the discretization of equations using methods like Runge–Kutta. This applicability extends to various systems, including the Lorentz map, the Lotka–Volterra system, and numerous other examples, and such applications deserve future and interesting investigations.

Author Contributions: The authors made equal contributions to the elaboration of this work. All authors have read and agreed to the published version of the manuscript.

Funding: R. da Silva expresses gratitude to CNPq for the financial support provided under grant number 304575/2022-4.

Conflicts of Interest: The authors declare no conflict of interest.

References

- Lichtenberg, A.J.; Leiberman, M.A. *Regular and Chaotic Dynamics*; Springer: Berlin/Heidelberg, Germany, 1992.
- da Silva, R.; Peretti, D.E.; Prado, S.D. Deterministic and stochastic aspects of the stability in an inverted pendulum under a generalized parametric excitation. *Appl. Math. Model.* **2016**, *40*, 10689. [[CrossRef](#)]
- Duchesne, B.; Fischer, C.W.; Gray, C.G.; Jeffrey, K.R. Chaos in the motion of an inverted pendulum: An undergraduate laboratory experiment. *Am. J. Phys.* **1991**, *59*, 987. [[CrossRef](#)]
- Wigner, E.P. On a class of analytic functions from the quantum theory of collisions. *Ann. Math.* **1951**, *53*, 36. [[CrossRef](#)]
- Wigner, E.P. Characteristic Vectors of Bordered Matrices With Infinite Dimensions. *Ann. Math.* **1955**, *62*, 548. [[CrossRef](#)]
- Dyson, F.J. Statistical Theory of the Energy Levels of Complex Systems. I. *J. Math. Phys.* **1962**, *3*, 140. [[CrossRef](#)]
- Wishart, J. The Generalised Product Moment Distribution in Samples from a Normal Multivariate Population. *Biometrika* **1928**, *20A*, 32. [[CrossRef](#)]
- da Silva, R. Random matrices theory elucidates the nonequilibrium critical phenomena. *Int. J. Mod. Phys. C* **2023**, *34*, 2350061. [[CrossRef](#)]
- da Silva, R.; Fernandes, H.C.M.; Venites Filho, E.; Prado, S.D.; Drugowich de Felicio, J.R. Mean-field criticality explained by random matrices theory. *Braz. J. Phys.* **2023**, *53*, 80. [[CrossRef](#)]
- Marchenko, V.A.; Pastur, L.A. Distribution of eigenvalues for some sets of random matrices. *Math. USSR Sb.* **1967**, *1*, 457. [[CrossRef](#)]
- Chirikov, B.V. A universal instability of many-dimensional oscillator systems. *Phys. Rep.* **1979**, *52*, 263. [[CrossRef](#)]
- Butusov, D.N.; Karimov, A.I.; Pyko, N.S.; Pyko, S.A.; Bogachev, M.I. Discrete chaotic maps obtained by symmetric integration. *Phys. A* **2018**, *509*, 955. [[CrossRef](#)]
- Mehta, M.L. *Random Matrices*; Academic Press: Boston, MA, USA, 1991.
- Sinai, Y.; Soshnikov, A. Central limit theorem for traces of large random symmetric matrices with independent matrix elements. *Bol. Soc. Bras. Mat.-Bull./Braz. Math. Soc.* **1998**, *29*, 1. [[CrossRef](#)]
- Guhr, T.; Müller-Groeling, A.; Weidenmüller, H.A. Random-matrix theories in quantum physics: Common concepts. *Phys. Rep.* **1998**, *299*, 189. [[CrossRef](#)]
- Vinayak; Seligman, T.H. Time series, correlation matrices and random matrix models. In *AIP Conference Proceedings*; American Institute of Physics: College Park, MD, USA, 2014; Volume 1575, pp. 196–217.

17. Boaretto, B.R.; Budzinski, R.C.; Rossi, K.L.; Prado, T.L.; Lopes, S.R.; Masoller, C. Discriminating chaotic and stochastic time series using permutation entropy and artificial neural networks. *Sci. Rep.* **2021**, *11*, 15789. [[CrossRef](#)]
18. Frahm, K.M.; Shepelyansky, D.L. Diffusion and localization for the Chirikov typical map. *Phys. Rev. E* **2009**, *80*, 016210. [[CrossRef](#)] [[PubMed](#)]
19. Tarnopolski, M. Correlation between the Hurst exponent and the maximal Lyapunov exponent: Examining some low-dimensional conservative maps. *Phys. A* **2018**, *490*, 834. [[CrossRef](#)]
20. Manchein, C.; Beims, M.W. Conservative generalized bifurcation diagrams. *Phys. Lett. A* **2013**, *377*, 789. [[CrossRef](#)]
21. Feigenbaum, M.J. Quantitative universality for a class of nonlinear transformations. *J. Stat. Phys.* **1978**, *19*, 25–52. [[CrossRef](#)]
22. Metropolis, N.; Stein, M.L.; Stein, P.R. On finite limit sets for transformations on the unit interval. *J. Comb. Theor.* **1973**, *15*, 25. [[CrossRef](#)]

Disclaimer/Publisher’s Note: The statements, opinions and data contained in all publications are solely those of the individual author(s) and contributor(s) and not of MDPI and/or the editor(s). MDPI and/or the editor(s) disclaim responsibility for any injury to people or property resulting from any ideas, methods, instructions or products referred to in the content.